*34th EPS Conference on Plasma Phys. Warsaw, 2 - 6 July 2007 ECA Vol.**31F**, P-2.146 (2007)*

Localized temperature and velocity measurements of C VI ions using active CXRS spectroscopy in the TJ-II stellarator

J. M. Carmona, K. J. McCarthy, R. Balbín, V. Tribaldos, M. Ochando, F. Medina and TJ-II Team
Laboratorio Nacional de Fusión, Asociación EURATOM-CIEMAT, E-28040 Madrid, Spain

Introduction

An active charge-exchange recombination spectroscopy (CXRS) diagnostic, based around a diagnostic neutral beam injector (DNBI) and a bidirectional (two vertical opposing views) multi-channel spectroscopic system, has been set-up on the TJ-II, a four-period [1], low magnetic shear, stellarator. It provides 5 ms long pulses, up to two per discharge, of neutral hydrogen accelerated to 30 keV with equivalent current of 3.3 equ. A. The bidirectional diagnostic is designed to measure Doppler shifts and widths of the C VI line at λ = 529.06 nm in up to 3 arrays of 12 channels with ~1 cm spatial resolution across the plasma minor radius [2]. The light dispersion element is a Holospec spectrograph with three 100 μm curved entrance slits (these are curved to compensate for its short focal length) and a transmission grating sandwiched between two BK7 prisms. It provides a focal-plane dispersion of ~11.5 Å/mm at 529 nm. Moreover, a narrow bandpass filter centred on 529 nm prevents spectral overlapping from the multiple fibre arrays at the image plane. The set-up includes a high-efficiency back-illuminated CCD camera and fast mechanical shutter ($\geq$4.5 ms time window). With on-chip binning, multiple spectra can be collected during discharges ($\leq$300 ms). Finally, fibre alignment was performed by illuminating each fibre bundle with a bright light source and observing, through an unused viewport, the orientation and location of the resultant bright spots with respect to markings on the inside of the opposing vacuum flange. In this way, the sightlines through plasmas can be determined using a cross-sectional machine drawing and magnetic configuration maps. Finally, when compared with the neutral beam geometry the normalized radius, ρ, corresponding to each beam/line-of-sight interaction volume is found.

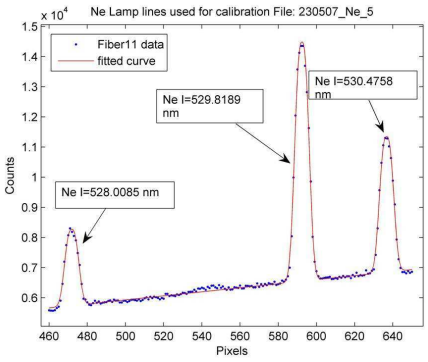

Fig.1 Ne I lines about 529.06 nm

Instrument calibration

Wavelength calibration and the instrumental function are obtained for all fibre channels between discharges using a pencil type Neon lamp located in front of fibre bundle head. For

this, wavelength calibration is performed using a second order (polynomial) fit to three nearby Ne I lines (Fig.1). As spectra are recorded simultaneously for all fibres in an array, fine corrections can be made for any nonlinear dispersion in the spectrometer or displacement error in the entrance slits. The instrument function is determined using a Gaussian function fitting. It is found to be ~7.6 pixels (~1.14 Å) and ~6.3 pixels (~0.95 Å) for the central fibres of the middle and short wavelength arrays. Fig. 2 illustrates the full-widths at half maximum (FWHM) of the fibres along the middle array. The variation across the array can be accounted for by small variations in width along the entrance slit, introduced during manufacture, rather than by changes in the vertical focussing of the spectrograph. It should be stated that the Ne I lines were fitted with a Gaussian function using a nonlinear least squares algorithm. Also comparisons were made between robust and non-robust fitting algorithms. In general, robust algorithms are generally considered better than non-robust ones as robust ones are less sensitive to outlier points (they are measurements numerically distant from the rest that can lead to misleading fits). However, it was found that robust fits show significant fibre-to-fibre variations for both FWHMs (Fig.2.) and line centres whilst non robust fits provided more stable behaviour. In certain cases robust methods may result in better fits when single Gaussian fits are done, but they prove to be weak when multiple Gaussian fits are performed, as in our case. Hence, the non robust method is chosen as our default fitting method. In addition, a comparison was performed using several data sets (frames) to confirm that the variations, which were small, were due to statistical variations in the Ne lines and not to the fitting procedure or to spectrograph anomalies. These showed such differences to be $\leq 5 \times 10^{-4}$ nm (Fig.3).

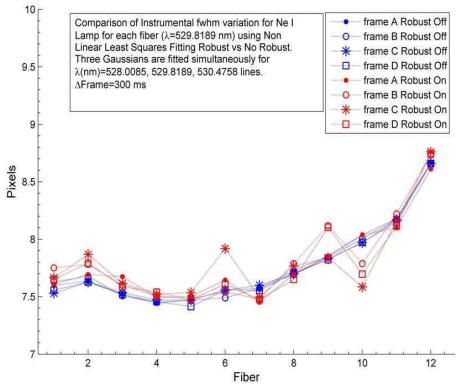

Fig.2. Variation of instrumental FWHM along the middle fibres for robust and nonrobust methods

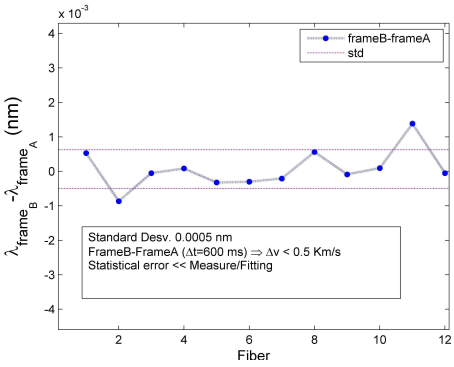

Fig.3. Differences in Ne I line centre between frames

Active and passive signals

The advantage between active and passive spectroscopy, is the localization of the emission. Passive measurements are line integrated and require inversion codes to obtain localized

information (the more lines-of-sight, the more precise the inversion). In addition, an accurate knowledge of the emissivity profile is needed (usually obtained by inversion) which can in turn lead to large propagation of errors. As localization is intrinsic in active measurements, CXRS is widely used to obtain spatially resolved measurements, although it presents several challenges [3]. For instance, active signals can be weak for certain plasma conditions, precise alignment of the neutral injector beam (heating or dedicated diagnostic injector) and collection optics as well as a reliable means to separate active and passive signals are needed. As the mean-wavelength of CVI line could change for different plasma conditions, an accurate way to determining this mean-wavelength (to calculate Doppler velocities) is to use opposite facing fibres looking at the same point, and then using the wavelength separation between their line centres ($\lambda_0^{CVI} = \lambda_1 + (\lambda_2 - \lambda_1)/2$) to find this mean-wavelength.

Spectra analysis tool

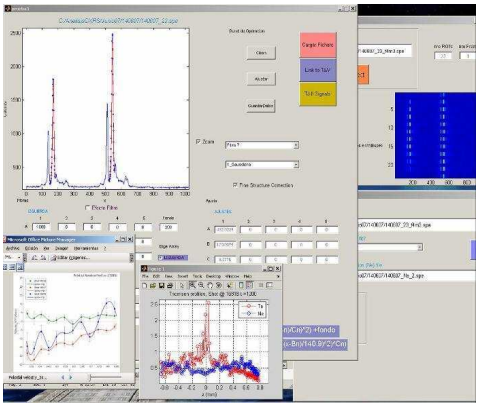

Fig.4. Interface screen for analysis

In order to process the large amounts of data (for instance, 12 “double” spectra per frame, 5 frames per discharge and 40 discharges by day provides about 2400 spectra per day plus calibration data), a user-friendly semi-automated tool for spectra analysis was developed in a Matlab environment. Fits to spectral lines are done using a nonlinear least squares algorithm (using a trust on region optimization method). Indeed, fits using up to 5 Gaussians are easily performed. Moreover options, such as the inclusion of a bandpass filter profile or fine structure corrections to the C^{+5} line, are available. For this an analysis is first made of the calibration data (Ne lamp spectra) to obtain the dispersion, instrumental function (FWHM) and a second order calibration function for each fibre. Then, a fit is made to the line of interest (i.e. C^{+5}) for each fibre and a Doppler shift and width are estimated together with error estimates.

Fine structure in C VI data

A detailed analysis of C VI spectral data was made in order to identify possible line asymmetries, contamination lines, etc. For this passive data were analysed in the first instance. This revealed a clear asymmetric about the C^{+5} line (see Fig.5) due to fine structure in the transitions in this hydrogen-like ion [4, 5]. Indeed, there are up to 13 possible lines with different intensities depending on plasma conditions. Moreover, these differ for transitions originating from charge exchange between neutrals and fully-stripped carbon and from

electron impact ionization. Fine structure lines are shown with relative intensities for CX in

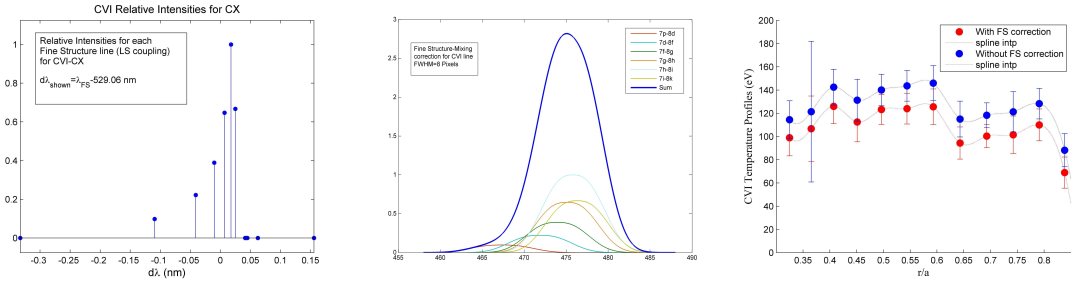

Fig.5 Fine structure transitions for CVI (8→7) and apparent temperature correction

Fig.5 where they show the clear non-symmetric tail (on the short wavelength side) that results in apparent line broadening.

CXRS measurements

First CXRS measurements have been performed on the TJ-II using the set-up described before (Fig.6). Hydrogen plasmas were created and heated with up to 600 kW of 2nd harmonic X-mode ECRH on lithium preconditioned walls. Plasmas with electron densities of the order 0.65 x 10^{19} m^{-3} and lasting 250 ms were studied. This discharge length allowed several CCD frames to be collected. In order to separate passive and active C VI signals discharges were selected where the electron density and temperature were constant. The resultant profiles of impurity ion temperature and velocity obtained with the analysis tool are shown in Fig.6. These first measurements show a dependence of the poloidal rotation profile on the ECRH heating conditions, and ion temperatures similar to those obtained with the NPA diagnostic [6], thus giving us confidence on the diagnostic operation. In conclusion, the diagnostic is now ready to operate and further studies will be carried out in the near future.

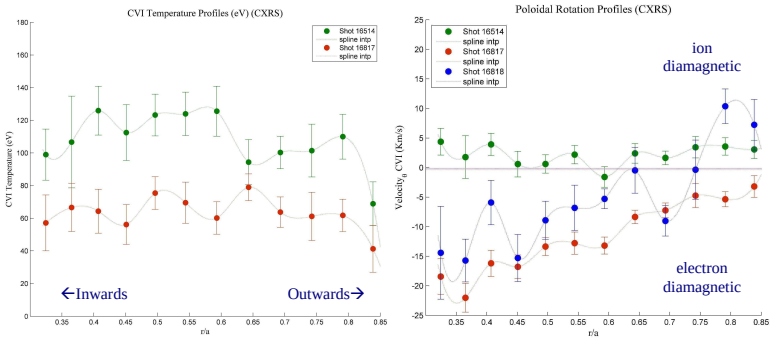

Fig.6. Ion temperature and poloidal velocity profiles for ECRH plasmas with <Ne>=0.65 x 10^{19} m^{-3}

References;
[1] E. Ascasíbar *et al.*, Fusion Eng. Des. **56-57**, 145 (2001).
[2] J.M. Carmona *et al.*, Rev. Sci. Instrum. **77** (2006) 10F107.
[3] R. C. Isler *et al.*, Phys.Rev. A **24** (1981) 2701
[4] R. J. Fonck, Phys. Rev. A **29**, 3288 (1984).
[5] K. Ida *et al.*, Rev. Sci. Instrum. **71** (2000) 2360.
[6] R. Balbín *et al.*, 15th Inter. Stellarator Workshop, Madrid (2005)